Large-displacement symmetrical foldable cones

K. A. Seffen*

Advanced Structures Group, Department of Engineering, University of Cambridge, CB2 1PZ, United Kingdom

(Received 27 May 2021; accepted 7 October 2021; published 2 November 2021)

A foldable cone, or f-cone, is a discrete vertex folded from flat with curved faces, and is an exemplar of nonrigid origami. We determine the exact equilibrium shape of a well-folded symmetrical f-cone by geometrical considerations alone, by treating as cones intersecting along original fold lines expressing equal fold angles. When moderate displacements prevail, the shape is found alternatively from the spherical image of the vertex, from deploying Gauss's mapping. The analytical working is much less compared to direct linearization of the exact solution framework; expressions for shape parameters are availed in closed form, and some of their variation is accurately retained compared to the exact case.

DOI: 10.1103/PhysRevE.104.055001

I. INTRODUCTION

Figure 1 shows several homemade disk structures, which combine folding and elastic curving in an obvious way. A thin steel shim is folded plastically in half in Fig. 1(a) to form a shallow inverted ridge line, which is then pushed through, and upwards, at its center point. The ridge line pops and folds in the middle, into a vertex with two conical halves connected across the original ridge-line fold angle.

If paper card is used instead, the ridge line is more flexible and can unfold when forming the vertex. Being paper, however, it is much easier to adjust the ridge-line fold angle, for example by pinching the ridge line shut with glue to give more pronounced conical portions: see Fig. 1(b). Upside-down versions, in metal and in paper card, Figs. 1(c) and 1(d), have the same shapes when folding is equivalent, which suggests a dominating geometrical character, independent of material choice.

The original disk can obviously be folded more than once to form an immediate apex, with conical faces extending outwardly, cf. the twice-folded symmetrical disk in Fig. 1(e). Steel, again, ensures near-rigid fold angles, which prevail when the vertex is pushed though to form another but shallower conical form.

These motifs are commonly known as foldable cones, or f-cones for obvious reasons, and first coined in Ref. [1]. They are also bistable structures, simply made, with two standalone shapes; only the singly folded case has plane facets initially.

They were devised as the simplest exemplars of nonrigid origami vertices. Traditional origami has, for decades, inspired the design of deployable structures, which unfurl by the relative opening of flat facets, hinged together around vertices in the folded state. Applications include solar panel membranes, antennae surfaces, and a variety of expandable and collapsible tubes [2].

A foldable vertex must be kinematically mobile, which first sets conditions upon the layout and operation of the hinge lines around it (assuming the hinges themselves to be singular lines and freely articulating) [3]. Ideally, the material thickness is zero, otherwise free motion is stymied by facets possibly colliding and thence deforming. From knowledge of spherical mechanisms, alternative thick-walled mobile vertices can be synthesized by placing the hinge lines on different planes through the facet thickness [4].

Each f-cone here is created from a single planar disk, where hinge lines are strictly folded lines with elastic resistance relative to some initial fold angle [5]; thin paper card avails low resistance while metal shim folds are near rigid in comparison. Because each fold line must also fold again in half to form the apex of vertex, material stresses are, thus, singularly concentrated at the apex in both directions of folding, which may restrict natural formation of the apex shape. Even if fold lines and the apex can articulate freely, an f-cone is never an ideal mechanism because there is always deformation during folding; rather, it is a compliant mechanism.[1]

Irrespective of fold-line behavior, the proponents of f-cones originally studied the relationship between folding, deformation, and bistability, assuming fold angles to be specified parameters and the apex of vertex to be formed freely. Two particular folding schemes were considered, with equal levels of folding in the same sense, as in Fig. 1 (and the object of study here), or folded alternatively in opposite directions, and with different fold angles in either sense; this second scheme reduces the conical deformation for the same level of folding compared to the first.

Conical, i.e., inextensible deformation is realistic from using thin sheets; and, correspondingly, simplifies displacements for a tractable analysis. A variational approach in Ref. [1] establishes a final governing equation of moderate displacements, which is then solved in closed form. Boundary conditions are the displacement gradients along the edges of

*kas14@cam.ac.uk

[1]Strictly, it is a compliant shell mechanism [6].

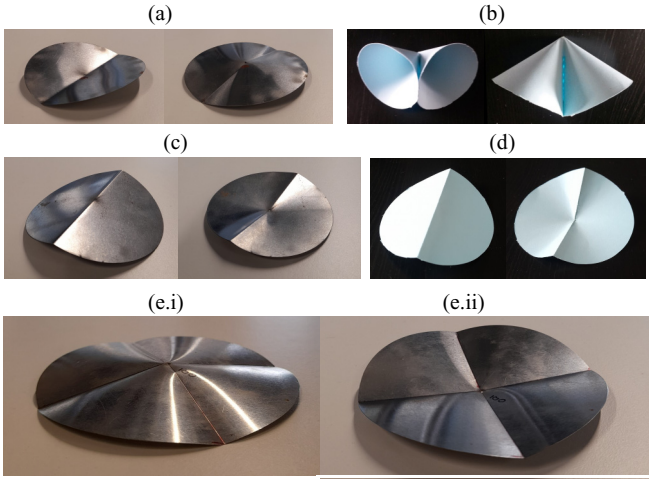

FIG. 1. Foldable cones, or f-cones, made from disks of steel shim (a), (c), (e) or paper card (b), (d) folded once, (a)–(d), $n = 2$, or twice, (e), $n = 4$. In (a) and (c), the planar folded disk is pushed through and upwards to form two conical portions on each side of the fold line; (c) is (a) in upside-down views. The fold line in (b) is fully creased, with the conical halves meeting tangentially on the line; (d) has the same shape as (c), in paper card. The twice-folded disk in (e.i) is pushed through and downwards to form the shape in (e.ii); both vertices are conically curved.

shallow conical portions, equal in size to the specified fold-line angles; and, originating in a Lagrangian multiplier, a fixed angular separation of fold lines in plan view to account for portions being connected to each other. Analysis was subsequently enhanced to include nonsymmetrical layouts of fold lines and large-displacement behavior in Ref. [7], in which exact solutions of shapes for different folding schemes are furnished as special elliptic functions of conical curvature.

The latter reminds us of the elastica solution for heavily curved beams [8], which are also couched as elliptic functions, except for the case of uniform bending under equal and opposite moments applied to the beam ends, which is a simple geometrical solution.

Equal folding delivers the same outcome for an f-cone, in surface terms. Its exact shape thus comprises identical, spatially uniform overlapping cones, which intersect radially along the fold lines, where the rotation between the local tangent planes is equal to the fold angle. This boundary condition can be fulfilled by geometrical algebra alone, with solution parameters as familiar conical shape terms such as the angle of its apex, etc. Large rotations can be captured in closed form, cf. the numerical approach needed in Ref. [7], and is one solution aim here; we also show that bistable solutions are inverted shapes for the same level, and direction, of folding.

We arrive at a set of coupled trigonometric expressions that are solved implicitly for a specified fold angle. The degree of coupling, however, does not easily avail direct expressions, say, for moderate displacements from setting small rotations and gradients. This is desirable because it provides a compact linear basis written explicitly in closed form despite some loss in accuracy. There are, of course, such descriptions from Ref. [1] but they do not express a uniformly curved shape for equal folding. Rather, enforcement of the Lagrangian multiplier leads to in-plane forces, which induce extra, nonuniform bending moments.

These forces are an artifact of the assumptions in Ref. [1] for the approach taken. In particular, the width of each conical portion between fold lines is reduced after rotating away from horizontal contrary to the Lagrangian multiplier operation; a second-order geometrical incompatibility is generated, which leads to in-plane forces. The formulation is thus overconstrained but it is not erroneous: fictitious boundary conditions are common as a worthy compromise for a solving advantage, e.g., Mansfield's inextensional theory [9].

We therefore turn to a different scheme, founded upon the origami premise of vertex folding. From Gauss's *theorema egregium* [10], any such vertex has zero angular defect and is said to be developable. Gauss also proves that the angular defect is equal to the area of its spherical image, which is a closed figure formed by mapping the orientation of the surface around the vertex onto a sphere of unit radius. The image of any developable vertex therefore has zero net area, which sets a determinate relationship between the level of folding and overall shape.

Constructing the spherical image of an f-cone is straightforward but evaluating zero net area must invoke rules of spherical trigonometry, which are formidable at times; this is not a worthy exercise given that the outcome will match our exact geometrical solution. The corresponding image for moderate displacements is, however, more simply configured as a planar figure from assuming shallow gradients, as directed originally in Ref. [11]. Obtaining the linearized solution from the exact case is automatically conveyed by evaluating its area conventionally. Furthermore, other f-cone properties of shape are directly expressed from its spherical image, which is worthy of comment.

The layout of this paper is as follows. Interconnected beam elasticae are presented first in Sec. II as an introductory geometrical analogy for f-cone behavior. Our two solution schemes, the exact conical geometry and shallow spherical image, then consider the simplest (singly folded) f-cone together in Secs. III and IV, respectively, before dealing with general f-cones in Secs. V and VI. On the latter, there is naturally more complexity and detail—and two conically folded (bistable) states to account for: one upright and one inverted. We present all results in Sec. VII, and new directions of study are noted in our final discussions, Sec. VIII.

II. BEAM ELASTICAE

Equal and opposite bending moments, M, are applied to a pair of straight beams in Fig. 2(a), which become ostensibly curved and mirrored. The angle 2θ subtended by a uniform radius of curvature, R, can be reexpressed, if required, in terms of M, a bending stiffness B, and a beam length l as $\theta = l/2R = Ml/2B$.

The curved beams are brought together and slotted into rotational fixtures. The applied moments are now internalized, with the fixtures simulating a pair of permanent, symmetrical folds in an elastica ring of arc length $2l$.

The folded semiangle is μ, equal to $\theta - \pi/2$ (or $\theta = \mu + \pi/2$); while a trivial expression, the level of folding and compatible curving are thus unique. An upper limit sets μ

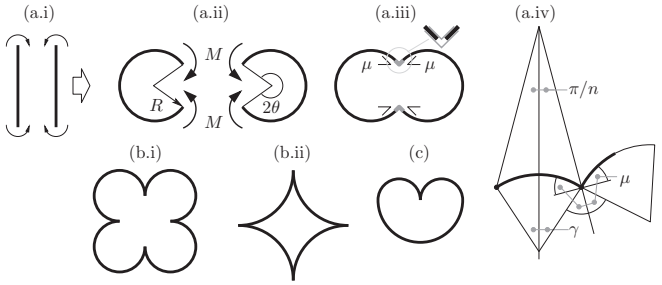

FIG. 2. Beam analogy for combined folding and curving of an f-cone vertex: (a.i)–(a.iii); a pair of uniformly curved beams locked together in rotational end fixtures, equivalent to $n = 2$; (a.iv) local geometry of a general beam segment where μ, in particular, is the fixture semiangle. (b.i), (b.ii) Two geometrically compatible configurations when $\mu = \pi/2$ (fully creased) for $n = 4$; (c) a beam reconnected to itself ($\mu = \pi/2$, arbitrarily) has nonuniform curvature, equivalent to a single radial fold line in an f-cone ($n = 1$).

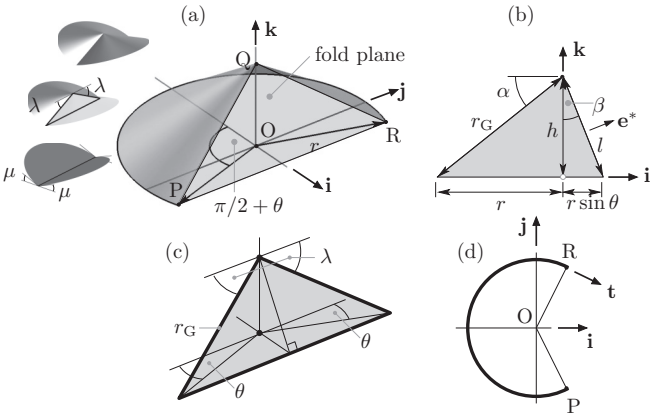

FIG. 3. Conical geometry of a singly folded f-cone vertex ($n = 2$). (a) Conical half, with its base resting horizontally and subtending $\pi + 2\theta$ radians; μ is the semiangle of the fold line, and λ, the vertex semiangle. (b) Vertical (**i**, **k**) plane through cone indicating apex semiangle, α, and other auxiliary parameters. (c) PQR plane isolated from (a); (d) conical base locus from (a) showing tangential unit vector, **t**.

equal to $\pi/2$ when the beams ends in both fixtures are parallel, i.e., fully creased. Setting $\mu = -\pi/2$ restores straightness.

A general arrangement has n identical beams interconnected by equal fixtures. Each beam portion subtends $2\pi/n$, with its center of curvature lying inside the ring. The pertinent triangle in Fig. 2(a.iv) has the same μ and θ definitions as before, where summing interior angles to π returns $\mu = \theta - \pi/n$.

A second inverted configuration has each center of beam curvature lying outside, where $\mu = \theta + \pi/n$. Moving between the two states (if manufactured) may be achieved by twisting the entire ring out of plane with, presumably, a classical bistable snapping through. The fully creased shapes for $n = 4$ are shown in Figs 2(b.i) and 2(b.ii), where $\theta = \pi/2 \pm \pi/4$. The ring outline clearly resembles a cross-sectional, horizontal slice through the four-sided vertex in Fig. 1(e.i).

When $n = 1$, a single beam is curved and reconnected to itself by a single fixture, see Fig. 2(c). The final shape cannot be uniformly curved although end moments must be applied to maintain a specified fold angle; its ends must also be prised apart by collinear forces before slotting into the fixture. The bending moments around the ring are no longer constant but are solved as an elastica elliptic function. Axial forces are thus present in nonsymmetrically folded scenarios.

III. BASIC F-CONE: $n = 2$

The folded shapes in Figs. 1(a)–1(d) can be characterized entirely by properties of the single fold line: the semiangle of the vertex measured along the fold line, denoted by λ; and the folded semiangle across it, μ. The disk deforms on either side to form geometrically compatible conical halves.

The left-side conical half is excised and tilted so that its base rests horizontally in Fig. 3(a). This partial, open cone sits upright, with its apex Q located vertically above the origin of a coordinate system, O: the plane PQR divides both halves of the original f-cone, and is our vertex fold plane.

The uniform radius of the cone base is r and subtends an angle of $\pi + 2\theta$ radians from P to R, i.e., an increase of 2θ relative to the flat half. The original radius of the flat disk is now a geodesic radius, r_G, extending from the apex to every point on the base: e.g., $QP = QR = r_G$.

Orthogonal fixed unit vectors **i** and **j** lie in the horizontal plane, **k** is vertical, and altogether they form a right-handed set. A symmetrical vertical plane is specified by **j**, and the cone, with the fold plane, is tilted by a positive angle β along $-\mathbf{j}$.

The side view in Fig. 3(b) also indicates the semiangle of cone apex, α, its vertical height h above O, and an intrinsic length l extending from Q normal to PR. There is also an auxiliary unit vector $\mathbf{e}^*$ acting normally to the PQR plane such that $\mathbf{e}^* = \mathbf{i}\cos\beta + \mathbf{k}\sin\beta$.

The triangular opening formed by PQR shrinks as folding is increased, up to a closing limit of $\theta = \pi/2$ or a fully creased limit of $\mu = \pi/2$, whichever occurs first. Note that the vertex semiangle, λ, is also the inclination of QP, or QR, relative to the horizontal within the PQR plane; see Fig. 3(c).

In the (**i**, **j**) plane in Fig. 3(d), we see the base outline of cone and a tangential unit vector, **t**, at R equal to $\mathbf{i}\cos\theta - \mathbf{j}\sin\theta$. This vector also lies in the plane tangential to QR, which is rotated from the fold plane by μ. The evaluation formally uses the scalar dot product:

$$\mathbf{t}\cdot\mathbf{e}^* = \cos\mu \quad\rightarrow\quad \cos\mu = \cos\theta\cos\beta. \tag{1}$$

We can substitute for β by observing from Fig. 3(b) that $\cos\beta = h/l$ and $l^2 = h^2 + r^2\sin^2\theta$. For the cone itself, $h/r = \tan\alpha$ and $r/r_G = \cos\alpha$; and inextensibility of the arc length of base returns $(\pi + 2\theta)r = \pi r_G$.

Eliminating r/r_G and β between expressions and noting from the PQR triangle in Fig. 3(c) that $\cos\lambda = r\cos\theta/r_G$, we ultimately find:

$$\begin{aligned}\cos\alpha &= 1/(1 + 2\theta/\pi);\\ \cos\mu &= \cos\theta/(1 + \sin^2\theta/\tan^2\alpha)^{1/2};\\ \cos\lambda &= \cos\theta\cos\alpha.\end{aligned} \tag{2}$$

Their ordering is deliberate for solving purposes, which cannot relate μ and λ explicitly. Instead $\cos\alpha$ is computed from a specified nonzero value of θ, from which we find $\tan\alpha$. Both θ and α values are substituted into the second and third expressions above, in order to unite μ and λ implicitly.

We can determine a range of solution values, as if varying the fold angle: this is conveyed later with some general f-cone results but we first note two solution cases. Equation (1) is satisfied simultaneously by the limiting conditions $\mu = \pi/2$ and $\theta = \pi/2$. A fully folded (*viz.* fully creased) f-cone thus comprises two closed conical portions, which glance each other on a single vertical line ($\lambda = 90^\circ$). The corresponding apex semiangles from Eq. (2) are 30°, which is also the value for β, and their conical shapes can now be drawn alongside the earlier informal experiments (as part of a general set) in Fig. 11(a), to convey their similarities.

At the other extreme we assume a small fold angle (μ) for a linearized solution along with small values of α, θ and λ. Rewriting the (first) inextensibility condition in Eq. (2), we obtain:

$$\theta = \frac{\pi}{2}\cdot\frac{1-\cos\alpha}{\cos\alpha} \approx \frac{\pi}{2}\cdot\frac{1-(1-\alpha^2/2)}{1-\alpha^2/2} \approx \frac{\pi\alpha^2}{4} \qquad (3)$$

after setting $\cos\alpha \approx 1-\alpha^2/2$ from its series expansion.

In the second expression in Eq. (2), $\sin\theta \approx \theta$ and $\tan\alpha \approx \alpha$. Assuming that $\cos(..)$ is always written as $1-(..)^2/2$ when $(..)$ is much less unity, then

$$1-\mu^2/2 \approx \frac{1-\theta^2/2}{(1+\theta^2/\alpha^2)^{1/2}} \approx \frac{1-\pi^2\alpha^4/32}{1+\pi^2\alpha^2/32} \qquad (4)$$

from using Eq. (3) and noting from the binomial theorem that $(1+[..])^{1/2} \approx 1+[..]/2$. The top line approaches unity faster than the bottom and may be set equal to unity outright; the bottom line can be brought up top using the binomial again, i.e.,

$$1-\mu^2/2 \approx \frac{1}{1+\pi^2\alpha^2/32} \approx 1-\pi^2\alpha^2/32 \quad\rightarrow\quad \mu = (\pi/4)\cdot\alpha. \qquad (5)$$

The final expression in Eq. (2) is also written in terms of series expansions to yield $\lambda^2 = \alpha^2+\theta^2$. Replacing θ with Eq. (3), taking the square root and employing the binomial theorem, we find $\lambda \approx \alpha(1+\pi^2\alpha^2/32)$. Ignoring small higher-order terms compared to unity, then:

$$\lambda \approx \alpha \quad\rightarrow\quad \mu = (\pi/4)\cdot\lambda. \qquad (6)$$

A final linear expression is fortuitous despite the second-order dependency of θ upon α; the relative simplicity of terms has enabled us to make sensible judgments about which terms prevail or otherwise. Equation (6) is now obtained by a different route, with much less algebra.

IV. SPHERICAL IMAGE: $n = 2$

The folded f-cone shape is drawn again in Fig. 4(a.i). A sample set of unit vectors normal to its surface are labeled $1\ldots6$ and circulate in an anticlockwise direction around the apex. In plan view in Fig. 4(a.ii) their nominal inclinations away from vertical are indicated schematically.

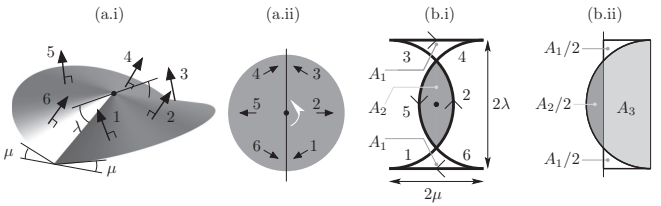

FIG. 4. Spherical image construction for singly folded f-cone vertex. (a.i) Some unit vectors, 1–6, normally appended to the vertex surface, circulating anticlockwise; (a.ii) schematic orientation in plan view. (b.i) Planar projection of corresponding spherical image for shallow displacements: the north pole (black dot) is the vertex apex; each curved path is semicircular, and the circulation follows the unit vector sequence in (a). Three areas enclosed by the profile in (b.i): A_1, twice (white), and A_2 (gray); (b.ii) is half of the image again, A_3 is an auxiliary area.

The spherical image arises from mapping normal unit vectors onto the surface of a unit sphere with the same normal orientation to produce a closed figure around the vertex. Relative to the apex unit normal at the north pole, $1\ldots6$ are located by their relative inclinations: "1" is thus south-westerly, "2" easterly, etc.

The image clusters around the pole when gradients are shallow and is practically flat, as drawn in Fig. 4(b.i). The path taken from 1 to 3 through 2 is a circular arc because the underlying cone is uniformly curved; this is reflected about a vertical pole line in plan view for $4\ldots6$. The center of curvature of each arc is displaced horizontally from the pole when each conical portion tilts inwards to the fold plane.

Moving across the fold line beyond 3 to meet 4 (and from 6 to 1), there is an abrupt reversal in surface gradient equal to the total fold angle, 2μ. Both arcs are now connected by horizontal lines of length 2μ assuming no change in the angle subtended radially by each conical half, i.e., π radians and $\theta = 0$.

The fold angle across the vertex pole, 2λ, is found equivalently from a unit normal traversing the apex within a vertical plane. This normal bisects the "3" and "4" normals initially and thus starts midway on 3–4 before finishing at the center of 6–1; this length is the image height in plan view.

There are two crossing points in the completed image, which separate three distinct areal portions: A_1 top and bottom, enclosed clockwise, and A_2 in between, anticlockwise. These areas oppose in the sense of their sign, allowing for zero area in accordance with Gauss's inextensibility requirement by setting $2A_1 = A_2$. There are rectangular and semicircular features, and noting the extra area, A_3, colored in Fig. 4(b.ii):

$$A_3 + 2\times(A_1/2) = \mu\cdot 2\lambda;\quad A_3 + A_2/2 = \pi\lambda^2/2. \qquad (7)$$

Eliminating A_3, we find:

$$2\mu\lambda - \pi\lambda^2/2 = A_1 - A_2/2 = 0 \quad\rightarrow\quad \mu = (\pi/4)\cdot\lambda \qquad (8)$$

as per Eq. (6).

The linear expression is plotted alongside the exact solution from Eqs. (2) in Fig. 10(a), and other results calculated later. There is practically no difference in performance up to $\mu \approx 0.5$ radians before then diverging.

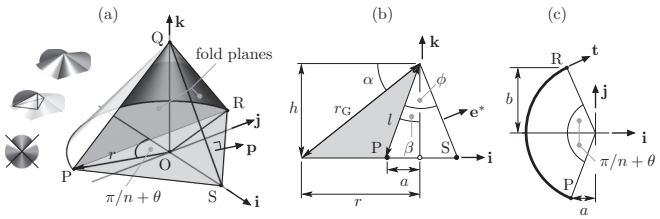

FIG. 5. Conical geometry of f-cone with n radial fold lines ($n = 4$, arbitrarily). (a) Single conical portion, (b) vertical slice plane, (c) base locus; and various auxiliary geometrical parameters.

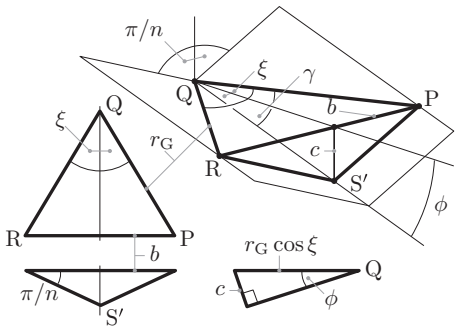

FIG. 6. Geometry of prism from Fig. 5. Note that S′ differs from S because the plane PRS′ is normal to QS.

Compared to the analytical linear solution in Eq. (3), θ has been zero, as noted. Accounting for nonzero θ would change the image by lengthening the semicircular arcs and connecting them with gently curved arcs for the fold angles, instead of straight. Such refinement adds $(1+\pi)\cdot(\theta/2)$ to the prefactor in Eq. (6), i.e., a negligibly small change, which does not alter the fundamental linear result.

V. GENERAL F-CONE: $n > 2$

An n-sided f-cone has n radial fold lines originally separated by $2\pi/n$ radians. When n is even, there are $n/2$ diametral fold lines, otherwise, each fold line is half of a traditional fold line for n odd.

The upright state corresponds to the apex pointing upwards, and vice versa during bistable inversion; and the fold lines are always folded as valleys with the same fold angle. Each conical portion deforms between two vertical planes passing through adjacent fold lines, which, together with the vertical pole axis and the horizontal plane, form bounding triangles, see Fig. 5(a).

A general upright conical portion is also shown in Fig. 5(a), which has been tilted to the horizontal. Some definitions are the same as Fig. 3: the uniform base radius is r, the conical apex semiangle is α, Fig. 5(b), and the geodesic conical radius from the apex is r_G. The fixed set of orthogonal unit vectors remains, as do points P, Q, and R on the cone.

The angle subtended by r is now $2\pi/n + 2\theta$ but drawn in Fig. 5(a) to be less than π; we account for being larger than π later. Inextensibility of the base arc-length sets $r/r_G = 1/(1 + n\theta/\pi)$, which is also equal to $\cos\alpha$ from Fig. 5(b).

The conical surface therefore lies behind the **j**, **k** plane, with the PQR plane rotated by β along **j** in Fig. 5(b). From auxiliary parameters a, h and l, $\cos\beta = h/l$ and $l^2 = a^2 + h^2$. In Fig. 5(c) we see $a = r\cos(\pi/n + \theta)$, whence $\cos\beta = 1/(1 + \cos^2(\pi/n + \theta)/\tan^2\alpha)^{1/2}$. The original f-cone vertical axis also tilts to become QS, where S is a new point on the **i** axis and rotated from PQR by ϕ, as shown: a normal unit vector in a vertical plane, $\mathbf{e}^*$, is written as $\mathbf{i}\cos(\phi-\beta) + \mathbf{k}\sin(\phi-\beta)$.

QPS and QSR are thus the tilted fold planes, with a unit vector, **p**, normal to the latter. Figure 5(c) indicates a horizontal tangent unit vector, $\mathbf{t} = \mathbf{i}\sin(\pi/n+\theta) + \mathbf{j}\cos(\pi/n+\theta)$, and the fold semiangle, μ, is thus calculated via $\cos\mu = \mathbf{t}\cdot\mathbf{p}$.

Looking along QS where the planes either side are rotated in true view by $2\pi/n$, we observe that **p** has relevant components $\mathbf{j}\cos(\pi/n)$ and $\mathbf{e}^*\sin(\pi/n)$. Hence:

$$\cos\mu = \mathbf{t}\cdot\mathbf{p} = \sin(\pi/n+\theta)\sin(\pi/n)\cos(\phi-\beta) + \cos(\pi/n+\theta)\cos(\pi/n). \quad (9)$$

An isolated prism resting on the fold planes in Fig. 6 with a face PRS′ normal to QS (S′ being different to S) provides auxiliary geometrical detail; in particular, two lengths, b (= PR/2, also shown in Fig. 5) and c, and two semiangles, ξ and γ, on the outside faces, where:

$$\sin\xi = b/r_G,\ \sin\gamma = \mathrm{S'P}/r_G,\ \cos(\pi/n) = \mathrm{c/S'P} \rightarrow b = r_G\sin\xi,\quad c = r_G\sin\gamma\cos(\pi/n). \quad (10)$$

Inside the prism, $\sin\phi = c/(r_G\cos\xi)$. Replacing c using the above: $\sin\phi = \sin\gamma\cos(\pi/n)/\cos\xi$. To express γ, we observe $\sin(\pi/n) = b/\mathrm{S'P}$ where, replacing b, $\sin\gamma = \sin\xi/\sin(\pi/n)$. Back substituting into $\sin\phi$ and tidying up: $\sin\phi = \tan\xi/\tan(\pi/n)$. From Fig. 5(c), $b = r\sin(\pi/n+\theta)$; thus $\sin\xi = \cos\alpha\sin(\pi/n+\theta)$.

Altogether, we have, in order of specification:

$$\cos\alpha = 1/(1+n\theta/\pi);$$
$$\cos\beta = 1/(1+\cos^2(\pi/n+\theta)/\tan^2\alpha)^{1/2};$$
$$\sin\xi = \cos\alpha\sin(\pi/n+\theta);\quad \sin\phi = \tan\xi/\tan(\pi/n). \quad (11)$$

For a specified value of θ, we may calculate ϕ and β, whence μ via Eq. (9).

The limit of θ is $\pi - \pi/n$ when the cone base wraps around completely by 2π radians. However, when $\theta > \pi/2 - \pi/n$, the conical portion subtends more than π radians, which alters the definitions of β and ϕ: see Fig. 7(a). Correspondingly, terms with $\phi - \beta$ in $\mathbf{e}^*$ and $\cos\mu$ are replaced by $\phi + \beta$; everything else remains the same.

The final f-cone shape is reassembled by first undoing the tilt of a conical portion, tantamount to rotating by $\phi - \beta$ along **j**, Figs. 7(b.i) and 7(b.ii), and restoring the f-cone axis as vertical. The new surface is then repeated $n-1$ times around **k** at intervals of $2\pi/n$, which effectively stitches each portion to the next along their fold lines.

The second, inverted arrangement maintains the same fold angle and thus follows the same geometrical assessment (all other terms remaining positive). However, restoring the tilted conical portion must replace ϕ by ϕ', see Fig. 7(c), where $\phi' = \pi - \phi$, in order to convey the inverted f-cone shape.

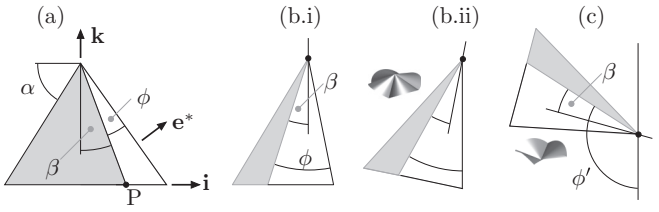

FIG. 7. (a) Vertical slice through conical portion, which subtends more than π radians; β and ϕ differ compared to Fig. 5(b). Restoration of conical portion, (b.i), by rotating its axis back to vertical, (b.ii), for an upright f-cone; (c) as (b) for inverted f-cone, ϕ' is equal to $\pi - \phi$.

Finally, the vertex semiangle, λ, has the same definition as before; of measuring the vertical angle of inclination of a fold line away from the horizontal. Calculating its value from the f-cone shape follows the scheme in Fig. 8 for the upright shape; for the inverted shape, ϕ is replaced by ϕ'. The f-cone fold lines form the inclined edges of a pyramid with two internal triangles highlighted, relating to ϕ and λ. Comparing their geometries yields:

$$\tan\lambda = \cos(\pi/n)/\tan\phi. \tag{12}$$

Before dealing with general results, we derive the linearized shape by extending the previous spherical image approach.

VI. SPHERICAL IMAGE: $n > 2$

Figure 9 conveys the spherical images for general folded upright and inverted f-cones (where $n = 3$ arbitrarily in the figure). The upright case is a straightforward extension of Fig. 4(b.i), with n circular arcs subtending $2\pi/n$ radians and interconnected continuously at their ends by fold-angle lines, 2μ, Fig. 9(a.i). The image has n exterior lobes attached to the corners of a curved interior core where the image crosses itself, and λ is measured from the pole point normal to the 2μ fold line.

Specific lobe and core geometry is detailed in Fig. 9(a.ii), where three areas are highlighted: A_1, half of the lobe area; A_2, $1/(2n)^{\text{th}}$ of the core area, which is equal to A_1 from Gauss's inextensibility requirement; and A_3, which completes the sector area with A_2. Each arc has a radius of curvature, ρ, equal to $\lambda + \mu/\tan(\pi/n)$ after inspecting the trapezium formed by adding A_1 and A_3. Its area, and that of the sector, are

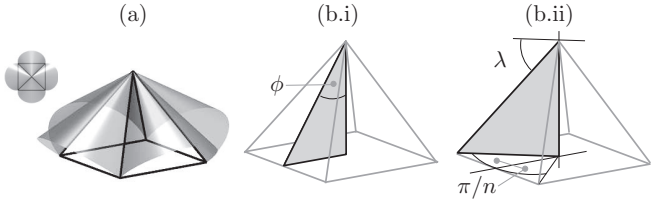

FIG. 8. (a) Fold lines of an f-cone forming the edges of a regular pyramid ($n = 4$, arbitrarily). Vertical pyramidal planes, (b.i) and (b.ii), for relating the vertex geometry between ϕ, λ, and n.

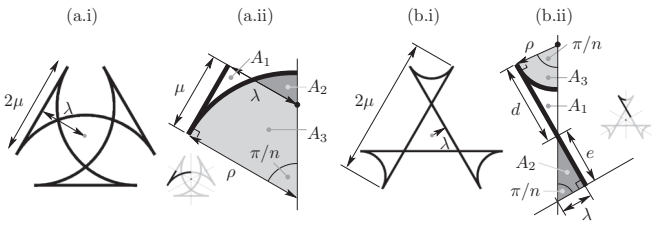

FIG. 9. Shallow spherical images for a general f-cone ($n = 3$, arbitrarily) when, (a), upright, and (b), inverted. Overall images are (a.i) and (b.i), with local areal detail in (a.ii) and (b.ii) respectively.

$$A_1 + A_3 = \lambda\mu + (1/2)\mu\cdot\mu/\tan(\pi/n);$$
$$A_2 + A_3 = (1/2)\rho^2(\pi/n). \tag{13}$$

Eliminating A_3 and setting $A_1 = A_2$, we find: $\lambda\mu + \mu^2/2/\tan(\pi/n) = (1/2)\rho^2(\pi/n)$. Substituting for ρ and rearranging into quadratic form:

$$\lambda^2(\pi/n)\tan^2(\pi/n) + \lambda\mu[2(\pi/n)\tan(\pi/n) - 2\tan^2(\pi/n)]$$
$$+\mu^2[\pi/n - \tan(\pi/n)] = 0, \tag{14}$$

which may be solved for the roots:

$$(\lambda/\mu)\cdot(\pi/n) = [1 - (\pi/n)/\tan(\pi/n)]$$
$$\pm[1 - (\pi/n)/\tan(\pi/n)]^{1/2}. \tag{15}$$

A positive value stems from selecting "+" under the ambiguous sign.

The image features swap places for the inverted f-cone; Fig. 9(b.i): the fold-angle lines now enclose the core portion and there is a sizable reduction in ρ and λ, comparatively. Slicing halfway through a lobe and some of the core, we obtain the outline in Fig. 9(b.ii) with highlighted areal portions: A_1 and A_2 deal with the lobe and core, A_3 is the sector area altogether.

Two auxiliary lengths, d and e, are also introduced, where $d + e = \mu$ and $\tan(\pi/n) = e/\lambda = d/\rho$. Correspondingly:

$$A_1 + A_3 = (1/2)\rho d;\quad A_2 = (1/2)e\lambda;\quad A_3 = (1/2)\rho^2(\pi/n). \tag{16}$$

Eliminating A_3 and setting $A_1 = A_2$, as per Gauss, $\rho d - \rho^2(\pi/n) = e\lambda$, which has the final quadratic expression (after

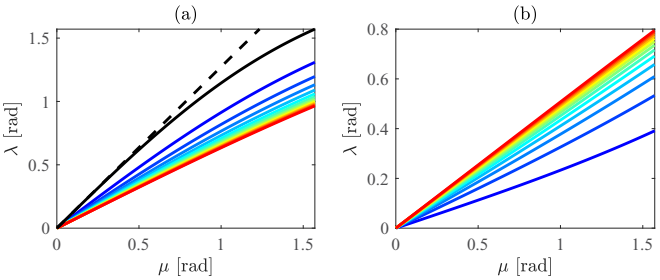

FIG. 10. Variation of f-cone vertex semiangle, λ, with fold angle, μ, for specified n (blue-to-red, $n = 3\ldots15$): (a) upright f-cones, (b) inverted. The solid black line, (a), is for $n = 2$; dashed line is Eq. (6), linear solution. (There is no inverted solution for $n = 2$.)

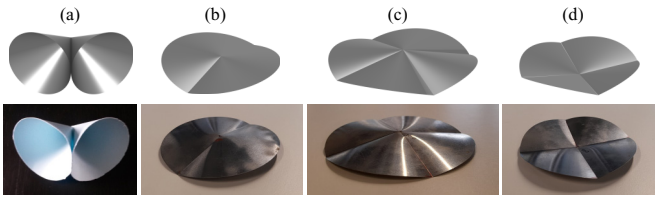

FIG. 11. Rendered shapes compared to models from Fig. 1. (a) $n = 2$ and $\mu = \pi/2$; (b) is much less folded; (c) and (d), the same upright and inverted f-cone.

some manipulation):

$$\lambda^2(\pi/n)\tan^2(\pi/n) - \lambda\mu[2(\pi/n)\tan(\pi/n) - 2\tan^2(\pi/n)] + \mu^2[\pi/n - \tan(\pi/n)] = 0. \quad (17)$$

Compared to Eq. (14), only the sign of the middle term differs, which changes the sign of root terms not their expressions. From the positive root the final relationships for both spherical images may be written:

$$(\lambda/\mu)_{(\text{upr, inv})} \cdot (\pi/n) = \mp[1 - (\pi/n)/\tan(\pi/n)] + [1 - (\pi/n)/\tan(\pi/n)]^{1/2}. \quad (18)$$

Finally note that ρ in both images is equivalent to the local apex semiangle of the conical portions. After some algebra, we ultimately find:

$$(\alpha/\mu)_{(\text{upr, inv})} = \pm(\lambda/\mu) + 1/\tan(\pi/n), \quad (19)$$

which, with other parameters, is now compared to exact solutions.

VII. PREDICTIONS

Values of λ and μ as a function of n in the range 3–15 (arbitrarily) are calculated using Eqs. (9), (11), and (12). Their variations are plotted in Figs. 10(a) and 10(b) for upright and inverted f-cones, respectively. The exact solution for $n = 2$ via Eqs. (2) is included in Fig. 10(a) along with the linear solution from Eq. (6).

The general trends for both orientations become more linear with n increasing. For a specific fold angle, an upright vertex becomes shallower, i.e., λ decreases; an inverted f-cone behaves oppositely but has smaller displacements from reduced levels of λ outright.

In both cases, the variations appear to converge to one another as n gets larger, albeit slowly: Eq. (18) suggests a limiting ratio for $\lambda/\mu \approx 1/\sqrt{3}$ when n tends to infinity; or $\lambda = 0.907$ when $\mu = \pi/2$, which appears to be accurate from calculating and plotting variations with a much higher limit of n.

Some f-cone shapes are rendered in Fig. 11 using MATLAB [12] to match the physical forms from Fig. 1. The latter's fold angles are measured crudely using a protractor in order to stipulate μ, and the rendered views aligned with them in the photographs. All shapes compare rather well.

A more formal assessment of the folded properties is delivered in Fig. 12 for upright f-cones and in Fig. 13 for their inverted states. Five final values of μ equal to μ_f are specified, from a moderate fold angle, $\pi/12$, to being fully creased, $\pi/2$ radians. We compute the corresponding final values of θ_f, α_f and λ_f over the previous range of n; values are normalized with respect to μ_f, for comparison.

For upright f-cones, θ_f/μ_f values increase with more folding but at slower rates with n. Starting values ($n = 3$) of θ_f/μ_f for inverted f-cones are always smaller, rise quickly with n before slowing.

Extra variations are plotted from linearizing the inextensibility expression from Eq. (11). Assuming a small apex semiangle, $\cos\alpha \approx 1 - \alpha^2/2$; using the binomial theorem and rearranging, we find:

$$\alpha^2 \approx 2n\theta/\pi \quad \rightarrow \quad (\theta/\mu) = (\alpha/\mu)^2 \cdot (\mu/2) \cdot (\pi/n) \quad (20)$$

with α/μ given by Eq. (19) after replacing λ/μ from Eq. (18): the subscript "f" is reintroduced. Note that θ above is not availed by the spherical image analysis, as discussed for the case of $n = 2$. Except for lowest μ_f, the trends are poorly captured linearly for upright f-cones, Fig. 12; but matters are reversed for inverted f-cones, Fig. 13, where initial (low n) behavior is rather good, and well maintained over n when μ_f assumes moderate values.

The apex semiangle trends with μ_f are reversed, with the largest ratios of α_f/μ_f occurring when folded the least; the rate of increase with n attenuates throughout. The linearized expressions, Eq. (19), are included, which, unsurprisingly, fare best when μ_f is lowest and the deformation is smallest.

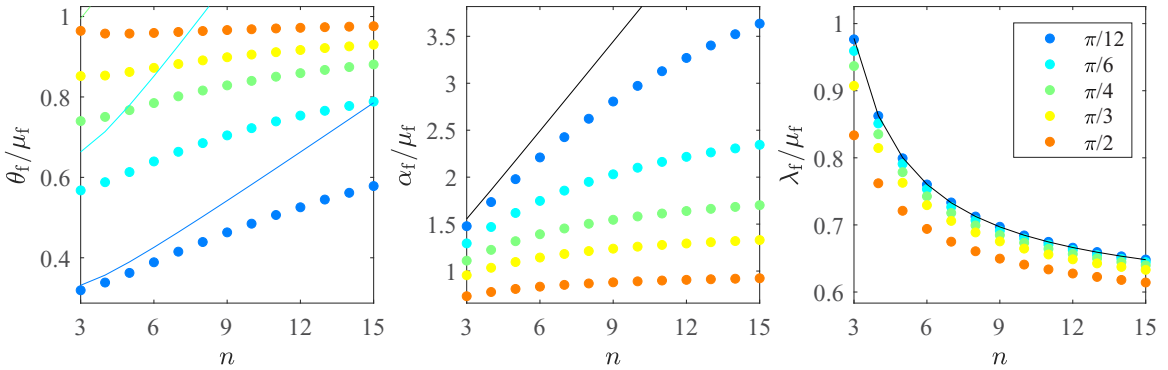

FIG. 12. Variation of final (subscript "f") parameters with n for specified fold angles ($\pi/12 \ldots \pi/2$) for upright f-cones. Dots are exact geometrical solutions, and curves are linearized solutions via Eqs. (20), (19), and (18), respectively.

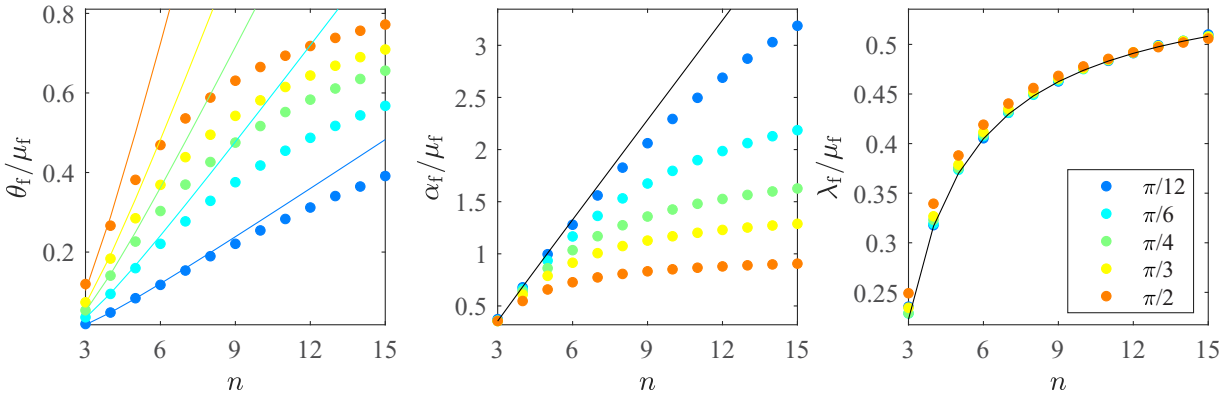

FIG. 13. As Fig. 12, for inverted f-cones.

Again, the comparison is better for inverted f-cones because their displacements are naturally smaller.

Finally, the variations of λ_f/μ_f with n oppose, with the ratio decreasing for upright cones and vice versa. Compared to θ_f and α_f, the trends are, however, closely packed—even converging altogether for inverted f-cones. The linearized predictions from Eq. (18) provide remarkably good boundaries on behavior, presumably from the near-linear behavior of exact solutions in Fig. 10.

VIII. DISCUSSION

We have argued that the shape of uniformly folded, inextensible f-cones depends only on their kinematical boundary conditions: we do not solve an equilibrium problem, rather, one of geometrical packaging. The exact conical shape stems from solving a set of coupled, nonlinear trigonometric (and algebraic) equations as a function of the number of fold lines and their level of folding; a principal output is the fold angle of the resulting vertex.

Because we assume developable folding, an exact spherical image via Gauss's mapping yields the same geometrical description: our equations resemble typical relationships from spherical trigonometry [13]. A planar approximation of this image, however, affords an alternative linearized solution describing shallow gradients from small fold angles, which commands less working. We have not directly compared our analysis to the seminal study in Ref. [1] because their shapes are not uniformly curved (but we expect any differences in shape predictions to be very small, for shallow displacements, at least).

A singly folded ($n = 2$) f-cone is a bistable structure with a flat-folded configuration and a single vertex state; otherwise ($n > 2$) f-cones are bistable vertices. An inverted f-cone has less conical deformation and a smaller vertex angle compared to the upright case folded the same. The more fold lines there are, the smaller the limit of vertex folding—because more conical portions are required to form.

The f-cone is also a type of conical defect, which can arise when thin-walled structures deform heavily [14]. In many related studies of defect shape, governing equations of deformed equilibrium are sought accordingly while embracing singular properties at the vertex of curvature and stress (*viz.* strain, bending strain energy density). Their success depends on capturing the true constitutive nature, elastic and inelastic, of whatever singular features arise, naturally or otherwise, and is a nontrivial exercise [5].

Because of symmetry and uniformity in our packaging approach, we can circumvent these difficulties and focus on the exact geometry. Variations on the vertex character are also simpler to propose and to study, for example, when there are nonuniform fold lines and fold angles, which admit, nevertheless, uniform shapes throughout. Taking inspiration from Fig. 2, we may start with interconnected beams of different lengths but uniformly curved, for example.

Furthermore, we refer to the fabric sculpture in Fig. 14. Clearly, this is an f-cone but one which cannot be laid flat; not because the fold lines are themselves curved, rather because the total angle subtended around the vertex appears to be well below 2π.

There is thus angular deficit and a corresponding spherical image with net area [10]. Even though it is not strictly developable from flat, the vertex can deform inextensibly once assembled from its individual pieces. There are now limits on the range of deformation compared to an ordinary f-cone, which may be revealed by having the deficit as an independent parameter when evaluating the spherical image area. We leave this exercise to the interested reader.

Finally, the packaging intent of f-cones is truly expressed only if the level of folding can be controlled, presumably

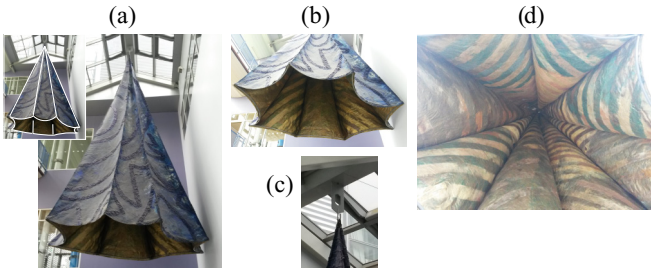

FIG. 14. Fabric f-cone artwork hanging in the Royal Victoria Hospital, Belfast (photographed by author circa July 2019). (a) Gently curved rods emanating from the apex, support a heavy fabric, hanging in conical sections; (b) base outline resembles the beam analogy from Fig. 2; (c) apex structural details; (d) axial view of pillowed interior.

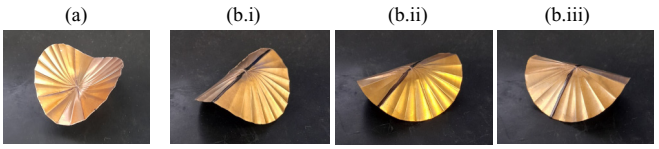

FIG. 15. Buckled f-cone made from thin copper beryllium sheet, whose unique ductility and hardness allow for many close fold lines ($n = 24$). No longer uniform but nearly cylindrical about a given axis, (a). This axis can be cycled around the disk almost neutrally, (b.i)–(b.iii); compare the cylindrical orientation to a fixed marker line (black) on the underside of disk (shown inverted).

by some external agency: our study, and that of others, establishes a snapshot of correspondingly viable conical deformation. But consider the folded metal disk in Fig. 15, made by the author over a decade earlier as a proof of concept for introducing residual bending prestresses in a simple way.

Rather than folding about successive diameters, each fold line is created by drawing a scribe tool along the diameter, which permits better control of how folding is imparted. Because folding is permanently set along many more lines than usual ($n = 24$, in this case), the interlineal spaces are imperceptibly curved (conically) but curved nevertheless, and the vertex shape rather weak.

The shape is, however, dominated by the prestresses, which approach the continuum case of uniform radial bending throughout. This is similar to the case of heating a bimetallic disk, which attempts to become doubly curved; but here, there is no circumferential bending intent, and thus interlineal conical bending can prevail to an extent. But like the heated disk, there is a threshold of folding extent (*viz.* heating levels [15]), which leads to a mode of near-developable, singly symmetrical displacements, as if the disk has buckled under progressive folding.

In Fig. 15 we therefore see an almost neutrally stable folded disk, whose shape can be circulated manually about a central axis with little resistance because of the general axisymmetry of the prestresses. From close inspection, local conical bending, however, remains, which presents an intriguing hierarchy of displacements compared to the overall shape, worthy of future study.

[1] F. Lechenault and M. Adda-Bedia, Generic Bistability in Creased Conical Surfaces, Phys. Rev. Lett. **115**, 235501 (2015).
[2] K. Miura and S. Pellegrino, *Forms and Concepts for Lightweight Structures* (Cambridge University Press, Cambridge, 2020).
[3] R. J. Lang, *Origami Design Secrets: Mathematical Methods for an Ancient Art* (A K Peters/CRC Press, Boca Raton, 2004).
[4] Y. Chen, R. Peng and Z. You, Origami of thick panels, Science **349**, 396 (2015).
[5] V. Brunck, F. Lechenault, A. Reid and M. Adda-Bedia, Elastic theory of origami-based metamaterials, Phys. Rev. E **93**, 033005 (2016).
[6] K. A. Seffen, Compliant shell mechanisms, Philos. Trans. R. Soc. **370**, 2010 (2012).
[7] I. Andrade-Silva, M. Adda-Bedia and M. A. Dias, Foldable cones as a framework for nonrigid origami, Phys. Rev. E **100**, 033003 (2019).
[8] R. Levien, *The Elastica: A Mathematical History*, Technical Report No. UCB/EECS-2008-103, University of California at Berkeley, 2008.
[9] E. H. Mansfield, *The Bending and Stretching of Plates* (Cambridge University Press, Cambridge, 1989).
[10] C. R. Calladine, *Theory of Shell Structures* (Cambridge University Press, Cambridge, 1983).
[11] S. M. Farmer and C. R. Calladine, Geometry of "Developable Cones", Int. J. Mech. Sci. **47**, 509 (2005).
[12] *MATLAB Release 2013b*, The MathWorks, Inc., Natick, Massachusetts, United States, 2013.
[13] I. Todhunter, *Spherical Trignometry* (Macmillan Publishers, New York, 1886).
[14] K. A. Seffen, Fundamental conical defects: The d-Cone, its e-Cone, and its p-Cone, Phys. Rev. E **94**, 013002 (2016).
[15] E. H. Mansfield, Bending, buckling and curling of a heated thin plate, Proc. R. Soc. London, A **268**, 316 (1962).